Received: 30 April 2021 | Revised: 10 January 2022 | Accepted: 14 January 2022

DOI: 10.1002/esp.5336

RESEARCH ARTICLE

ESPL WILEY

Debris flow initiation in postglacial terrain: Insights from shallow landslide initiation models and geomorphic mapping in Southeast Alaska

Annette I. Patton[1] | Joshua J. Roering[1] | Elijah Orland[2,3,4]

[1]Department of Earth Sciences, University of Oregon, Eugene, OR, USA

[2]University of Maryland Baltimore County, Baltimore, MD, USA

[3]Goddard Earth Sciences Technology and Research II, Baltimore, MD, USA

[4]Hydrological Sciences Laboratory, NASA Goddard Space Flight Center, Greenbelt, MD, USA

Correspondence
Annette I. Patton, Department of Earth Sciences, University of Oregon, Eugene, OR 97403, USA.
Email: patton.annette@gmail.com

Funding information
Sitka Sound Science Center (SSSC); National Science Foundation, Grant/Award Number: 1831770

Abstract

Debris flows pose persistent hazards and shape high-relief landscapes in diverse physiographic settings, but predicting the spatiotemporal occurrence of debris flows in postglacial topography remains challenging. To evaluate the debris flow process in high-relief postglacial terrain, we conducted a geomorphic investigation to characterize geologic, glacial, volcanic, and land use contributions to landslide initiation across Southeast Alaska. To evaluate controls on landslide (esp. debris flow) occurrence in Sitka, we used field observation, geomorphic mapping, landslide characteristics as documented in the Tongass National Forest inventory, and a novel application of the shallow landslide model SHALSTAB to postglacial terrain. A complex geomorphic history of glaciation and volcanic activity provides a template for spatially heterogeneous landslide occurrence. Landslide density across the region is highly variable, but debris flow density is high on south- or southeast-facing hillslopes where volcanic tephra soils are present and/or where timber harvest has occurred since 1900. High landslide density along the western coast of Baranof and Kruzof islands coincides with deposition of glacial sediment and thick tephra and exposure to extreme rainfall from atmospheric rivers on south-facing aspects but the relative contributions of these controls are unclear. Timber harvest has also been identified as an important control on landslide occurrence in the region. Focusing on a subset of geo-referenced landslides near Sitka, we used the SHALSTAB shallow landslide initiation model, which has been frequently applied in non-glacial terrain, to identify areas of high landslide potential in steep, convergent terrain. In a validation against mapped landslide polygons, the model significantly outperformed random guessing, with area under the curve (AUC) = 0.709 on a performance classification curve of true positives vs. false positives. This successful application of SHALSTAB demonstrates practical utility for hazards analysis in postglacial landscapes to mitigate risk to people and infrastructure.

1 | INTRODUCTION

Debris flows are recognized as a key process that shapes high-relief areas and can have devasting consequences for human safety, infrastructure, and the natural environment (Schuster & Highland, 2007). Debris flows travel rapidly through steep terrain, increasing their volume through entrainment, which can expand downslope areas of inundation and hazard zones (Hungr et al., 2005). Globally, debris flows have been documented in a wide array of settings, including forested steeplands, volcano flanks, breached moraine-dammed lakes, and postglacial alpine hillsides. As a result, the topographic and sedimentary signature of past debris flow activity can be highly diverse, emphasizing the need to characterize zones of debris flow initiation, runout, and deposition for hazards mitigation.

In soil-mantled steeplands (unglaciated), the repetitive action of shallow landslides that translate into debris flows imparts a distinctive and highly organized topographic signature over >10^6-year timescales (Stock & Dietrich, 2006). For example, in northern California and

western Oregon, steep, highly dissected headwaters with planform convergence generate shallow landslides that episodically sculpt downslope valleys (Benda & Dunne, 1997; Dietrich & Dunne, 1978). The resulting channel networks lack banks and other features typically associated with fluvial erosion. These so-called debris flow (or colluvial) networks, which often extend downvalley to valley slopes of 5–10%, constitute the vast majority of the valley network, highlighting their critical role in setting relief, erosion rates, and sediment delivery to the fluvial system (Stock & Dietrich, 2003). In these settings, physical and empirical models for shallow landslide initiation have been proposed and validated, providing geoscientists, land managers, and emergency personnel with tools for confronting spatial variability in debris flow hazard potential (Miller & Burnett, 2008; Montgomery & Dietrich, 1994).

By contrast, in postglacial landscapes, the recent and profound imprint of glacial erosion and deposition tends to dominate topography such that active landscape modification by an array of mass movement processes, including debris flows, does not match inherited topographic signatures (Brardinoni & Hassan, 2006). Nevertheless, the spatial distribution of colluvium, till, or other disaggregated sediments in postglacial terrain is a critical constraint on debris flow hazard potential (Bovis & Jakob, 1999; Brayshaw & Hassan, 2009) and sediment transport (Brardinoni et al., 2009, 2012). Similar to non-glacial landscapes, debris flows in glacial topography initiate on steep (>30°) hillslopes (Martin et al., 2002; Milne et al., 2015), but initiation points tend to occur in localized topographic depressions on otherwise planar hillslopes (Brardinoni et al., 2009; Milne et al., 2015) rather than well-established colluvial hollows that extend upstream of the fluvial network. Debris flows can also initiate on moraines or steep till-covered valley walls (Ballantyne, 2002b) and deposit large volumes of sediment in extensive fans where steep valley walls transition to low-gradient valley bottoms (Ballantyne, 2019). Debris flows are effective agents of erosion and transport on steep postglacial slopes (Ballantyne, 2019; Ballantyne & Benn, 1994; Hinchliffe & Ballantyne, 2009). In British Columbia, debris slides and flows transport an order of magnitude more sediment by volume to streams than other mass-wasting processes (e.g. creep and sheet wash) (Campbell & Church, 2003).

Because debris flows depend on the accumulation of unconsolidated material that becomes fluidized following destabilization (Iverson, 1997), the spatial distribution of glacial till, colluvium, or other disaggregated sediments in postglacial terrain serves as a critical constraint on hazard potential (Brardinoni et al., 2012). Furthermore, the runout of debris flows can be superimposed by chronic talus transport during paraglacial adjustment (Hinchliffe & Ballantyne, 2009), obscuring the paths of previous flows. As a result, the identification and characterization of landslide hazards can be challenging in postglacial terrain.

This contribution investigates controls on shallow landslide initiation in a steep, forested landscape modified by glacial erosion, tephra deposition, diverse microclimates, and variable land use. We address the spatial pattern of shallow landslides and debris flows across Southeast Alaska, focusing on Sitka, Alaska, a high-relief landscape where historic landslides threaten community safety.

Our approach incorporates data from a decades-long landslide inventory acquired by the US Forest Service in Tongass National Forest (TNF), and field and LiDAR-derived observations of geomorphic features. We also undertake a novel application of the shallow landslide model SHALSTAB (Dietrich et al., 2001; Montgomery & Dietrich, 1994) to postglacial landscapes to assess its predictive capability. This model is well supported in unglaciated terrain but untested in postglacial landscapes. Evaluating model performance in glaciated terrain is important on a practical level for hazards assessments in high-latitude postglacial landscapes. Our results provide a framework for communities to manage landslide hazards in postglacial settings.

2 | STUDY AREA: SITKA, SOUTHEAST ALASKA

We evaluated spatial patterns of landslide occurrence in Southeast Alaska and detailed investigation of the geomorphic history in the area near Sitka (Figure 1).

2.1 | Geologic and geomorphic history

Southeast Alaska is comprised of a structurally complex assemblage of accreted terranes (White et al., 2016). The NW–SE-striking Queen Charlotte–Fairweather fault system west of the study area accommodates much of the modern-day dextral motion of the Pacific Plate relative to Southeast Alaska (Elliott & Freymueller, 2020). On Baranof Island, Paleozoic metasedimentary and metavolcanic rocks of the Wrangellia Terrane are juxtaposed with Mesozoic–Cenozoic intrusive rocks and sedimentary rocks of the Baranof Accretionary Complex by a series of NW–SE-striking thrust and transform faults (Karl et al., 2015). The dominant bedrock near Sitka is a fractured Cretaceous graywacke.

Like much of Southeast Alaska, Baranof and the surrounding islands were heavily glaciated throughout the Pleistocene. Ice retreated from lowland coastal areas like Baranof Island by 12.1–12.4 ka (Ager et al., 2010; Hamilton, 1986; Kaufman & Manley, 2004; Mann, 1986; Mann & Hamilton, 1995). The region near Sitka is characterized by well-defined glacial valleys (Twenhofel, 1951) with steep walls and low-gradient valley bottoms. This high-relief terrain extends to the coastal margin of most of Baranof Island. Sitka Sound and other regions of Southeast Alaska lack systematic documentation of landforms and near-surface sediments.

Pleistocene–Holocene volcanic and sedimentary units overlie major bedrock contacts including ~12 ka glacial sediments (basal till, outwash, ice-contact deposits) and Pleistocene–Holocene volcanic flows and air-fall deposits (Karl et al., 2015; Riehle et al., 1992a,b). On large areas of Kruzof and Baranof islands, pyroclastic sediments were deposited in eruption events from the Mt. Edgecumbe Volcanic Field on Kruzof Island (Figure 1) (Riehle et al., 1992a). These eruptions occurred shortly after ice retreat, between 10.6 and 11.4 ka (Riehle et al., 1992b). Quaternary sedimentary deposits in Sitka are discontinuous due to original emplacement and subsequent heterogeneity in erosion patterns on till- and tephra-mantled hillslopes. Weathering of the Mt. Edgecumbe tephras during the Holocene has resulted in characteristically porous soil, as is typical of volcanic soils (Bommer et al., 2002; Greco et al., 2010; Nanzyo, 2002).

Human activity on Baranof Island has further modified the geomorphic landscape. Human settlement of Southeast Alaska may have begun as early as 17 ka (Lesnek et al., 2018). Beginning in the early

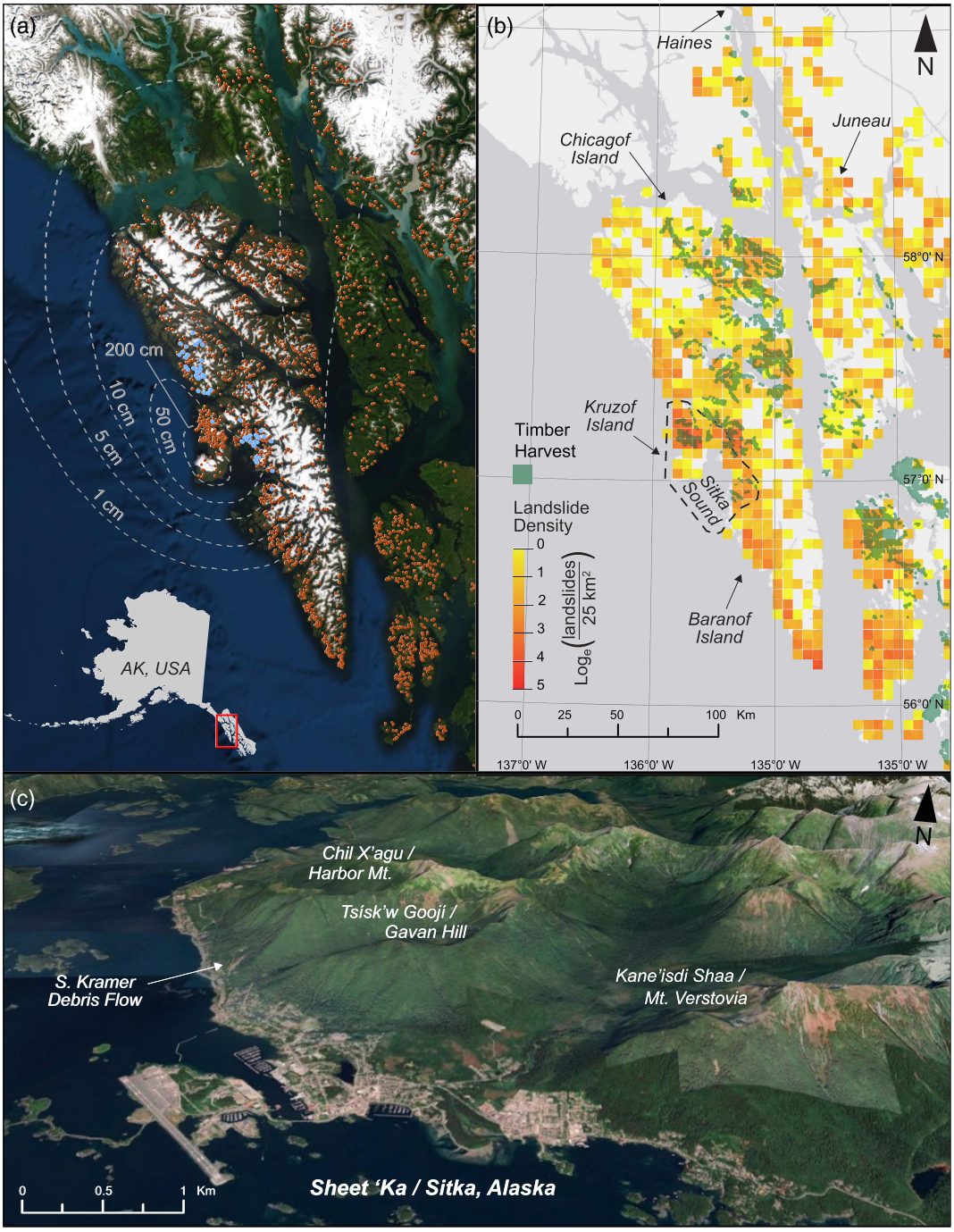

FIGURE 1 Study area in Southeast Alaska, USA. (a) Landslide initiation sites (red points) from the Tongass National Forest (TNF) landslide inventory on Baranof and the surrounding Islands. The inventory extends south and east of the region shown. Landslides that initiated during the 18 August 2015 AR are shown in blue. Mt. Edgecumbe isopachs are based on terrestrial tephra deposit mapping (Riehle et al., 1992a). (b) Natural log of landslide density (number of landslides per 25 km^2 grid cell) and location of Sitka Sound. Because the TNF landslide inventory spans a period of ~85 years, the highest density of landslides in the study area roughly translates to landslide frequencies of 0.02 landslides km^{-2} yr^{-1} (one landslide every 50 years per km^2). US Forest Service records document areas of timber harvest (green) since the 1900. (c) Oblique view of the town of Sitka, showing steep postglacial slopes and debris-flow channels on Harbor Mt., Gavan Hill, and Mt. Verstovia. Imagery from Google Earth [Color figure can be viewed at wileyonlinelibrary.com]

19th century, Russian colonists settled modern-day Sitka (Sandberg, 2013) and commenced extensive logging activities on Baranof and the many small islands in Sitka Sound (Heuer, 2020, personal communication). Timber harvest has continued throughout much of the last century, with records dating back to 1900 (Figure 1b).

2.2 | Climate and vegetation

Southeast Alaska is part of the world's largest temperate rain forest and is characterized by a mid-latitude maritime climate with high annual precipitation (Wendler et al., 2016). Particularly at low elevations along the coastlines, a majority of precipitation is rain. At sea

level in Sitka, mean annual precipitation during the last climatic normal (1981–2010) was 2205 mm/year.

Along the Pacific Coast, a majority of high-intensity rain storms and flooding events are controlled by landfalling atmospheric rivers (ARs) (Neiman et al., 2011). ARs are long (>2000 km), narrow (<1000 km), moisture-laden currents in the lower troposphere (Neiman et al., 2008; Ralph et al., 2004). When they encounter the steep topography of the coast ranges, orographic forcing results in high-intensity precipitation along the width of the AR (Neiman et al., 2011). Although diverse meteorological conditions may trigger landslides, ARs trigger a majority of shallow landslides in many areas of the western United States (Cordeira et al., 2019; Oakley et al., 2017) due to the high intensity and long duration of precipitation.

ARs in Alaska are an important process determining the patterns of storm precipitation along the Pacific Coast, including Southeast Alaska (Jacobs et al., 2016; Lavers et al., 2014; Sharma & Déry, 2020). In fact, ARs contribute up to 33% of annual precipitation and up to 90% of extreme precipitation in mountainous terrain near the coast of Southeast Alaska (Sharma & Déry, 2020). The contribution of ARs to rainfall totals is greatest in September and October, when ARs account for almost all extreme precipitation events in coastal areas like Sitka.

Southeast Alaska is densely forested, with over 50% forest cover (Van Hees & Mead, 2005) dominated by mixed conifer forests (Campbell et al., 2004) of western hemlock, Sitka spruce, western redcedar, Alaska cedar, and mountain hemlock (Harris & Farr, 1974). Disturbed and riparian areas host locally abundant red alder and black cottonwood. Non-forested regions include high-elevation tundra vegetation, surface water, glaciers, and snow/icefields (Kirchhoff et al., 2016).

2.3 | Landslides in Southeast Alaska

Following widely used classification systems (Cruden & Varnes, 1996; Hungr et al., 2014; Varnes, 1978), the term 'landslide' in this paper includes debris flows (rapid debris-laden flows that follow colluvial channels) and other landslide types. The majority of landslides in Southeast Alaska are debris flows initiated by shallow-seated landslides, with 87% of landslides classified as debris flows or unchannelized debris avalanches (Swanston & Marion, 1991). They typically occur in areas where convergent topography collects shallow groundwater. Landslides are particularly common on glacial hillslopes with a veneer of till or colluvial debris (Gomi et al., 2004; Swanston & Marion, 1991).

Like other areas in the western United States, landslides in Southeast Alaska tend to occur during high-intensity storms (ARs), particularly in areas where steep topography produces an orographic effect and/or where sub-linear valleys control the movement of storm cells (Swanston & Marion, 1991). Buma and Johnson (2015) also documented that high-intensity winds influence landslide initiation in Southeast Alaska.

Over the last 5–10 years, multiple ARs in Sitka have triggered debris flow and landslide initiation, including an unusually high-precipitation storm on 18 August 2015, which triggered >40 debris flows near Sitka (Busch et al., 2016; Landwehr et al., 2016). This storm demonstrated the potential for landslide hazards near Sitka, resulting in three fatalities and destroying valuable infrastructure (Figure 2a). The August 2015 storm demonstrated the extreme local variability in cumulative rainfall and maximum intensity, with heavy precipitation occurring within Sitka Sound and along the west coast of Baranof and Kruzof islands (Busch et al., 2016).

Landslides also pose hazards throughout Southeast Alaska (Figure 2). Multiple landslides have occurred in Juneau over the last 100+ years, including a debris flow in November 1936 that killed 15 people (Juneau Local Emergency Planning Commitee, 2009) (Figure 2e). Recent landslides in Haines (Figure 2d), which resulted in two fatalities and the destruction of eight homes (Jacobs, 2020), demonstrate the ongoing risk of AR-initiated landslides to isolated communities.

Much of the available understanding of landslide occurrence in Southeast Alaska comes from investigations of landslide initiation on logged hillslopes. On Prince of Wales Island (south of the primary study area), >50% of landslides that initiated during a storm in 1933 occurred in areas that had been logged in the previous year (Johnson et al., 2000). Timber harvest influences the frequency and size of landslides (Johnson et al., 2000; Swanston & Marion, 1991). Landslides in logged areas tend to be smaller and occur at lower elevations on shallower hillslope angles (Johnson et al., 2000). Areas where climate-driven ecological disturbances have impacted forest composition may also be more susceptible to landslide occurrence (Buma & Johnson, 2015). Even many years after forest disturbance, tree stand age influences debris flow mobility and runout length (Booth et al., 2020).

Channel development in Southeast Alaska is relatively young (<10 ka) compared to non-glaciated landscapes (Johnson et al., 2000). Instead, glacial ice dominated valleys until the late Pleistocene (Mann & Hamilton, 1995). Postglacial topography (wide, flat-bottomed valleys and a trellis drainage pattern) controls debris flow runout and deposition patterns (Gomi et al., 2004; Johnson et al., 2000). Debris is typically carried to the base of the slope as a debris flow, where low slope angles in valley bottoms and dense forest precipitate sediment deposition in fans. Only ~15% of debris flows deliver material directly to perennial streams (Swanston & Marion, 1991). When fine sediments and large wood are delivered to streams, such as in headwater channels (Gomi et al., 2004), these deposits have important implications for fisheries and aquatic habitats (Johnson et al., 2000).

3 | METHODS

3.1 | Landslide inventory in Southeast Alaska

To evaluate geomorphic and geologic controls on landslides, we characterized the distribution of landslides in Southeast Alaska and Sitka using the TNF landslide inventory (Tongass National Forest, n.d.). USFS scientists manually mapped >12 000 landslides using historical air photos and field investigations. Each mapped landslide has a polygon of landslide area and an initiation point. For each landslide, we calculated the polygon area and the aspect of initiation based on the Shuttle Radar Topography Mission (SRTM) version 2 digital elevation model, with spatial accuracy of 30 m, vertical accuracy of <16 m, and

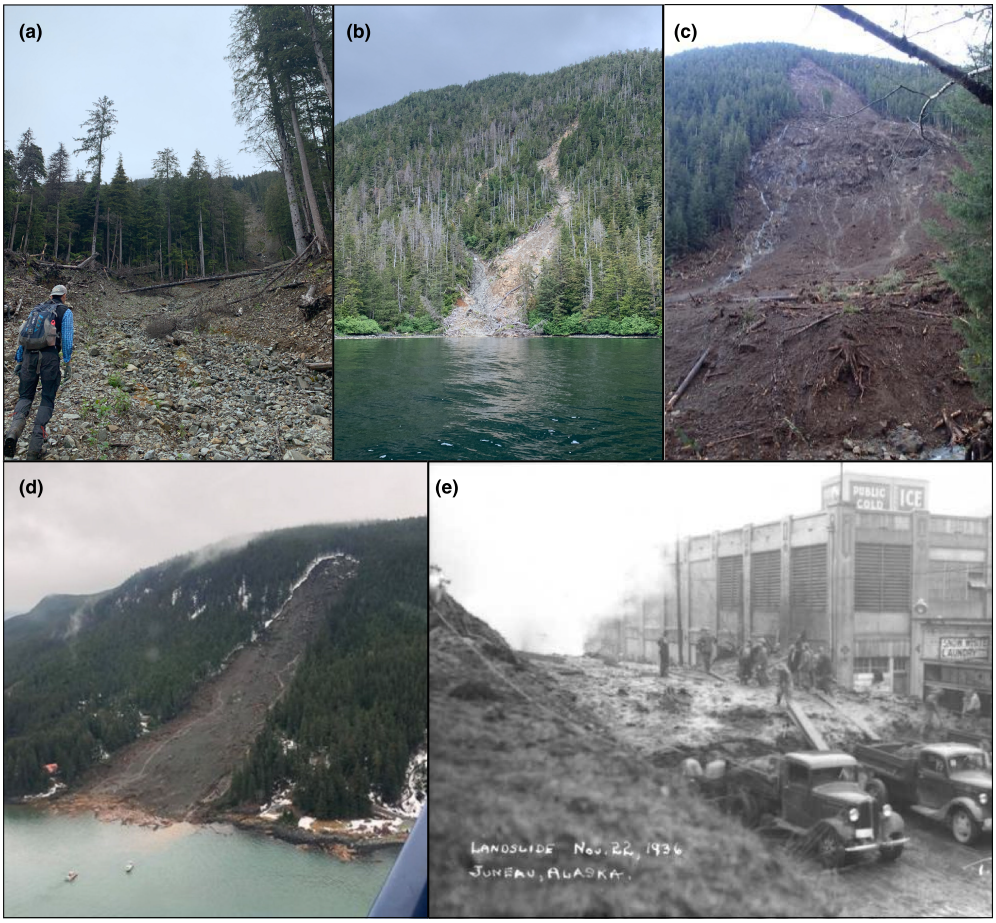

FIGURE 2 Examples of landslides in Southeast Alaska. (a) S. Kramer debris flow in Sitka, which initiated in August 2015 and killed three people. (b) A debris flow in Nakwasina Sound near Sitka, which initiated in August 2015. Debris flows are typical of landslides in the Sitka Sound. (c) The Starrigavan Landslide, which initiated in September 2014 and destroyed a bridge and other infrastructure. (d) A landslide in Haines, which initiated in December 2020 and killed two people. Photo from Alaska Public Media. (e) The toe of a landslide in downtown Juneau, which initiated in November 1936 and killed 15 people. Photo from Alaska State Library Historical Collections [Color figure can be viewed at wileyonlinelibrary.com]

tile resolution of 1°. We calculated spatial landslide density as the number of landslides per 25 km^2 grid cell across the entire area of the inventory.

To compare landslide distribution and characteristics in the Sitka area relative to the rest of Southeast Alaska, we subset the landslide inventory data based on geography. In order of descending geographic area, subset groups include the entire TNF landslide inventory, Baranof Island, the area near the Sitka Sound (Figure 1), and Kruzof Island. Notably, some of these subset groups overlap. For example, the TNF inventory includes all other landslide subsets, and the Sitka Sound subset includes landslides on Kruzof Island as well as some landslides on Baranof Island. Nevertheless, these subsets are useful in identifying regional patterns of landslide occurrence.

Limitations of the landslide inventory include potential bias in mapping landslides from air photos. For example, the inventory may be biased towards larger landslides (under-sampling) (Stark & Hovius, 2001), or landslides in areas where forest cover is less dense (Brardinoni et al., 2003; Steger et al., 2017; Turner et al., 2010), such as logged areas. Furthermore, the historical landslide inventory may not reflect changing climatic conditions (Coe & Godt, 2012; Patton et al., 2019) that are likely to affect current and future patterns of landslide initiation.

3.2 | High-resolution geomorphic mapping

To evaluate the control of local geology and geomorphology on the landslide regime in Southeast Alaska, we mapped the geomorphology of the hillslopes near Sitka. We identified surficial geomorphic units in the field based on bedrock/deposit characteristics and remotely using a 1 m airborne LiDAR digital elevation model (DEM) obtained by the Alaska Division of Geological & Geophysical Survey (DGGS) in 2018 (Daanen et al., 2020). We expanded upon the lithologic units previously mapped on Baranof Island (Karl et al., 2015) and added specificity to existing maps by documenting a previously unmapped conglomeratic member of the Sitka Graywacke Formation. We used the modified Varnes classification scheme to identify landslide-related geomorphic features (Cruden & Varnes, 1996; Hungr et al., 2014; Varnes, 1978). Other geomorphic units follow standard Quaternary mapping schemes (Compton, 1985), which align with the geo materials defined in the USGS Standards (2020), although specific unit names and symbols have been modified for brevity and visual clarity. Contacts (boundaries between units) were drawn at 1:10 000 according to field observation or remotely using high-resolution Google Earth imagery and the LiDAR DEM. We consider contacts that we

did not extensively validate in the field 'approximate', although detailed topographic data allow for high precision in mapping contacts between geomorphic units, which were observed in detail in the field. We further distinguished relevant geomorphic landforms, such as the presence of highly channelized hillslopes.

3.3 | Shallow landslide modelling and validation

To evaluate the applicability of a frequently used model for shallow landslide initiation in postglacial landscapes, we used the shallow landslide stability model, SHALSTAB, first introduced by Montgomery and Dietrich (1994). This model is specifically chosen because it offers an objective assessment of potential debris flow initiation sites based on topography alone. In essence, SHALSTAB identifies steep, convergent topographic landforms that tend to accumulate colluvial materials over timescales >100 years, exhibit elevated soil moisture, and focus shallow subsurface stormflow over sub-annual to hourly timescales. The implementation of SHALSTAB requires a DEM and raster processing software to use (Vieira et al., 2018). In this study, we used a combined 1 m and resampled 0.5 m-resolution LiDAR DEM collected and processed by the Alaska DGGS in 2018 (Daanen et al., 2020).

SHALSTAB provides a physically interpretable estimate of slope stability on a pixel-by-pixel basis according to the following relation, which results from the combination of a limit equilibrium slope stability model and a shallow groundwater flow model:

$$q_{cr}/T = [\sin\theta(\rho_s/\rho_w)(b/a)][1-(\tan\theta/\tan\varphi)]$$

where q_{cr} is the critical rainfall rate to induce failure; T is saturated soil transmissivity (assumed constant across the study area); θ is the ground surface slope; a is the upstream contributing area; b is the width of pixel; ρ_w and ρ_s are the bulk densities of water and soil, respectively; and φ is the angle of internal friction. Notably, this version of SHALSTAB does not account for heterogeneity of cohesion and soil transmissivity. Detailed derivation and parameter explanation can be found in Montgomery and Dietrich (1994) and Dietrich et al. (2001).

In applying this model to landscapes that lack model parameterization (Dietrich et al., 2001), the physical terms ρ_s and φ are assumed to be constant, set at 2000 kg/m^3 and 45°, respectively. We set the angle of internal friction to be artificially high (45°) to account for SHALSTAB's lack of explicit incorporation of root cohesion. Where the surface slope is greater than the angle of internal friction ($\theta > \varphi$), the output $q_{cr}/T < 0$. Such hillslopes are considered 'unconditionally unstable' (i.e. unstable in in any hydrologic condition). In previous studies, these areas are often observed to be too unstable to develop a colluvial mantle or soil and thus manifest as bare bedrock slopes or cliffs with little/no potential to initiate shallow landslides due to limited material available for slide initiation (e.g. DiBiase et al., 2017; Lamb et al., 2013). While these simplifications do not account for local heterogeneity, previous validation studies indicate that this simplified approach is an effective strategy to evaluate spatially distributed landslide potential (Dietrich et al., 1995, 2001).

The model output, q_{cr}/T, provides a measure of the normalized precipitation needed to induce slope failure at various locations across the landscape. Less intense critical rainfall values (i.e. lower q_{cr}/T) correspond to the most unstable parts of the landscape. Low q_{cr}/T values highlight areas with high slope relative to the internal friction angle (θ/φ) and/or topographic convergence with significant contributing area (a/b), such that even low-intensity rainfall can have an enhanced likelihood of triggering slope failure. Dietrich et al. (2001) found that $\ln(q_{cr}/T) < -3.1$ served as a useful threshold to identify the majority of mapped headscarp locations and that random placement of the same polygons in their study areas produced a significantly higher (more stable) distribution of model values.

Several studies have proposed non-physical (empirical) models that combine slope angle and topographic convergence to predict landslide locations (Chae et al., 2017; Miller & Burnett, 2008). These empirical models can offer an improvement over SHALSTAB, depending on how well existing landslide data represents ongoing and future initiation processes.

To evaluate the applicability of the model to postglacial landscapes, we compare model results to landslides from the TNF landslide inventory. We individually corrected the mapped landslides in the Sitka region by locating the initiation sites (specifically headscarps) that are well expressed in the LiDAR data. In most cases, the inventory landslides were mislocated by >10 m, likely due to georeferencing errors in the air photos used to map landslides.

In the Sitka region, our corrected landslide inventory includes 38 landslides, 8 of which occurred on unconditionally unstable slopes. To test whether low q_{cr}/T values correspond to landslide initiation zones in our study area, we follow a modified validation procedure utilized by Dietrich et al. (2001), comparing mapped landslide initiation sites (headscarp polygons) with the underlying q_{cr}/T values of the 30 *conditionally* unstable hillslopes. Because the pixel size of our LiDAR DEM is much smaller than the scale of landslide initiation zones, an individual headscarp polygon encloses numerous pixels, and thus q_{cr}/T values. To determine the relevant q_{cr}/T value for each polygon we used the q_{cr}/T value associated with the 5th percentile of the distribution enclosed by the polygon. We chose not to use the lowest value in order to avoid outliers associated with topographic errors, and we chose not to use the central tendency of q_{cr}/T values because landslides are a threshold phenomenon and thus often result from local extremes. As such, the 5th percentile value serves as a compromise between unstable extremes and unrepresentative mean values.

TABLE 1 Summary statistics for landslides in each of the geographic areas discussed below

	TNF	Baranof Island	Sitka Sound	Kruzof Island
Total region area (km^2)	68 000	5770	1920	672
No. landslides	12 013	936	447	280
Median landslide area (m^2)	6102	7090	3820	2791
Area interquartile range (m^2)	2574–13 427	3411–15 251	1729–8008	1224–6534

To test whether SHALSTAB identifies preferential locations of landslide initiation, we performed a Monte Carlo analysis by randomly scattering the 30 landslide polygons across the LiDAR data in landslide-prone areas (slopes > 25°) and calculating the 5th percentile of the underlying distribution of q_{cr}/T values. By comparing these 5th percentile q_{cr}/T values with those from the actual landslide locations, we can identify the extent to which SHALSTAB improves the identification of landslide initiation sites compared to random locations in steep terrain. Using the 30 landslide polygons, we randomly relocated each polygon on the study area hillslopes 200 times, each time extracting the 5th percentile q_{cr}/T value from the distribution enclosed by each landslide polygon. In doing so, we generated 6000 5th percentile q_{cr}/T values using the randomly placed landslide polygons. We then compared the distributions of mapped vs. randomly placed 5th percentile q_{cr}/T values to assess the efficacy of SHALSTAB predictions.

4 | RESULTS

4.1 | Landslide occurrence in Southeast Alaska

Landslides are prevalent throughout the TNF in Southeast Alaska (Table 1). Landslides are common on Kruzof Island, western Baranof Island, and Prince of Wales and the surrounding islands and in areas where at least 50 cm of tephra was deposited on steep hillslopes (Figure 1a) and areas where logging history may increase the density of shallow landslides (Figure 1b) (Bishop & Stevens, 1964; Johnson et al., 2000; Swanston & Marion, 1991). In particular, western Baranof Island and Kruzof Island exhibit a strong gradient of landslide density in the inventory (Figure 1b), with a high density of landslides on the western margins and relatively sparse landslides within the interior and eastern coast of Baranof Island. The high density of landslides on Kruzof and western Baranof islands and low density of landslides on eastern Baranof Island is a unique pattern in the TNF inventory and extends beyond the distribution of Mt. Edgecumbe tephra (Figure 1a) and recent logging operations (Figure 1b).

The underlying topography in Southeast Alaska demonstrates an NNE–SSW trend of hillslope aspects. Landslides in the TNF occur preferentially on south/southwest aspects (Figure 3a). This pattern aligns with the most prevalent direction of atmospheric rivers in Southeast Alaska (Harris, 1999; Sharma & Déry, 2019) and slope aspects of greatest tree damage/blowdown (Harris, 1999). Landslides on Kruzof Island ($n = 280$) and around the Sitka Sound ($n = 447$) tend to be smaller than landslides throughout the TNF ($n = 12\,013$), while landslides on all of Baranof Island ($n = 936$) tend to be larger (Figure 4).

4.2 | Geomorphic and geologic controls on landsliding

Within the Sitka Graywacke Formation (Karl et al., 2015), we observed both a sandy graywacke unit and a cobble conglomerate unit (Table 2, Figure 5). Fractures are prevalent throughout bedrock exposures; field observation and topographic data indicate a series of NW–SE faults in the study area. Limited field evidence indicates a dextral sense of motion, consistent with dextral transtensional faults on Baranof Island (Karl et al., 2015).

Our mapping of Quaternary sediment deposits and topographic landforms confirms that glacial, colluvial, and volcanic sediments create a complex and locally variable geomorphic template near Sitka (Figure 5). We observed both erosional and depositional glacial landforms in Sitka (Figure 5), including >1 m-thick till and outwash deposits in valley bottoms and erosional features (glacial polish and

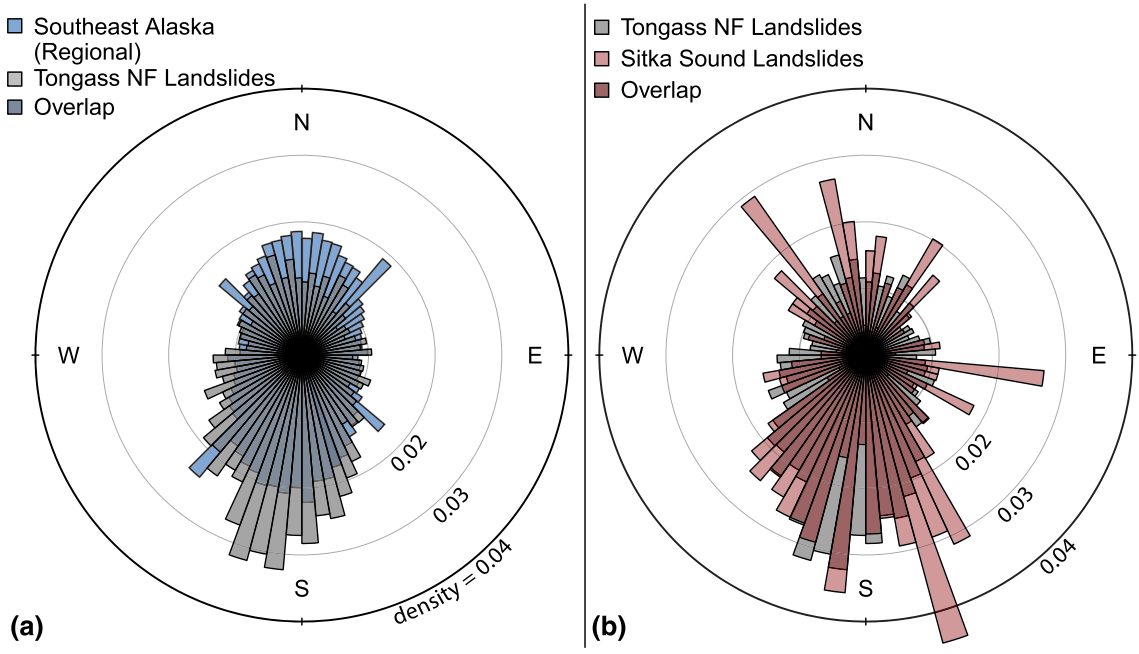

FIGURE 3 (a) Aspect of n = 12 013 landslides in the Tongass NF landslide inventory (gray) compared to the overall distribution of hillslope aspects in Southeast Alaska (blue) and (b) n = 447 landslides near the Sitka Sound (red) [Color figure can be viewed at wileyonlinelibrary.com]

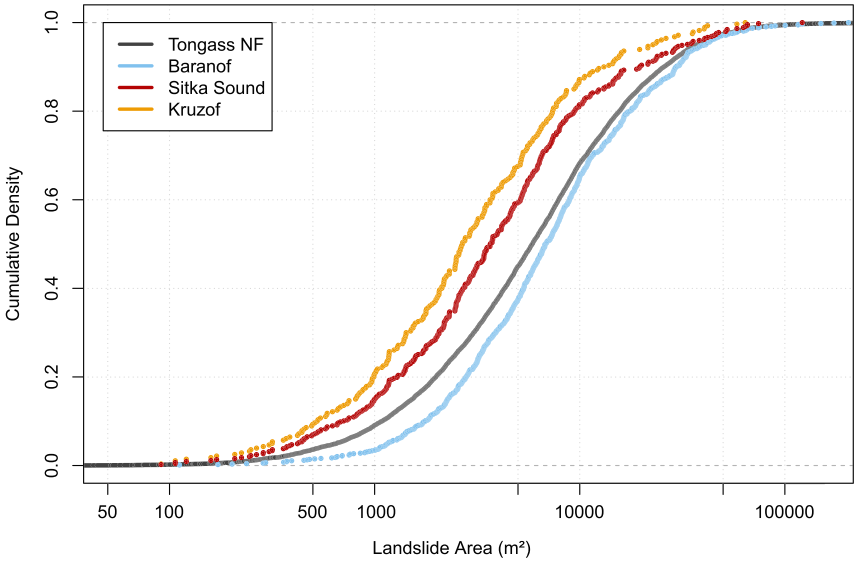

FIGURE 4 Observed distribution of landslide areas by geography. Landslides on Kruzof Island (n = 280) and around the Sitka Sound (n = 447) tend to be smaller than landslides throughout the Tongass National Forest (n = 12 013), while landslides on all of Baranof Island (n = 936) tend to be larger [Color figure can be viewed at wileyonlinelibrary.com]

TABLE 2 Description of geomorphic units, including both the primary lithologic units (symbolized with colour in Figure 5) as well as additional information about relevant landforms (symbolized with patterns in Figure 5). In addition to the surficial units displayed on the geomorphic map, Mt. Edgecumbe tephra is also prevalent across the map area (Figure 1) but its modern-day distribution is too discontinuous to display at this scale due to secondary erosion and reworking by hillslope processes. Intact (but patchy) tephra deposits are most commonly found on undisturbed ridgetops and buried beneath colluvial deposits at the toe of hillslopes

Landslide	Rapid mass-wasting features. Most landslides in the study area are debris flows that initiated as shallow landslides.	
Alluvium	Sorted, unconsolidated sediment of varying grain size, including sand and gravel deposits in active channels and floodplains.	
Beach deposits	Rounded sand and gravel in the wave-worked tidal zone.	
Debris flow fans	Debris flow deposits containing poorly sorted sediment in broad depositional zones where steep hillslopes transition into low-gradient valley bottoms. Debris flow fans may also include alluvial deposits but are characterized by predominantly debris flow sediments.	
Colluvium	Unsorted, unconsolidated coarse sediment on hillslopes. Grain size varies but colluvium in the study area is typically coarse (pebbles to boulders) and subangular. Colluvium includes talus material and mass-wasting material. Colluvium near Sitka typically contains abundant bright red, fine matrix, interpreted as reworked volcanic tephra.	
	Landform: channelized hillslopes	Erosional topography characterized by steep (>25°), planar, incised channels, including both fluvial channels (with likely debris flow influence) and debris flow (colluvial) channels. Fluvial channels experience perennial surface flow. Colluvial channels (more common) were observed to experience ephemeral surface flow.
	Landform: sediment wedge	Transitional topography where channels have incised into a wedge-like colluvial deposit, typically underlain by tephra and/or till. Based on channel depth, minimum combined sediment thickness appears to vary from 10^0 to 10^1 m.
Outwash	Relict sand and gravel deposits attributed to Pleistocene pro-glacial rivers.	
Glacially scoured surface	Smooth topography characteristic of glacial erosion. Polished/striated bedrock is locally exposed beneath patchy, thin till (<1 m) or tephra.	
Till	Unsorted glacial sediment. Deposits are patchy at variable scales and vary in thickness up to several metres, which may reflect both primary depositional patterns and subsequent erosion. Undisturbed deposits are characteristically grey/green in colour.	
Sitka graywacke (sandstone)	In the map area, the Sitka Graywacke is dominantly thick-bedded to massive lithic sandstone, indicative of inner fan depositional zones (Karl et al., 2015). Regionally, this unit is characterized by medium- to thin-bedded sandstone, siltstone, and mudstone turbidite deposits.	
	Landform: glacial imprint	A broad landform category that includes both erosional (glacial striations, glacial polish) and depositional features (discontinuous till deposits <1 m thick), indicating contact with glacial ice.
Sitka graywacke (conglomerate)	Thick-bedded to massive conglomerate, with rounded to sub-rounded clasts up to 30 cm in a sandy matrix.	

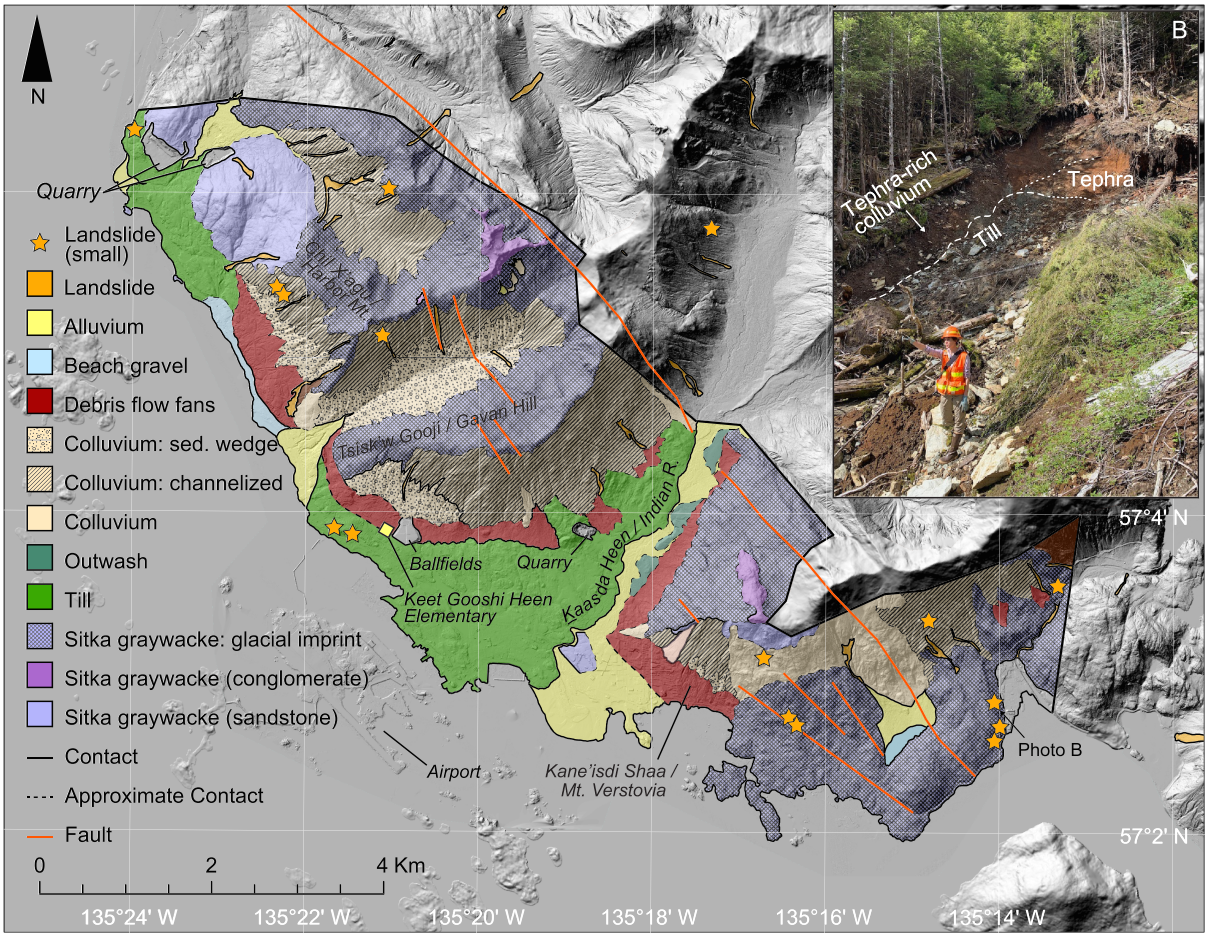

FIGURE 5 Geomorphic map of Sitka, including landslide areas modified from the Tongass National Forest landslide inventory. (B) Photo of the Sawmill Debris flow, which initiated along the tephra/till boundary in 2015. Mapping is based on extensive field observation, topographic evaluation, and existing map data. However, limited access and time constraints prevented field validation of every contact. Approximate contacts (dashed lines) were located using remote interpretation of lidar topography with some local field validation. Unit descriptions and interpretations are described in more detail in Table 2 [Color figure can be viewed at wileyonlinelibrary.com]

striations) at high elevations (<800 m), rocky coastal outcrops, and bedrock exposures in the southeast portion of the mapped area. Consistent with previous studies (Riehle et al., 1992a), discontinuous tephra deposits are typically 0.5–1 m thick and exist across the majority of the study area, except in areas of localized erosion, such as the channelized portions of the hillslope and active river channels.

Channelized colluvium and debris flow fans extend into the developed areas of Sitka. Inventoried landslides initiated in multiple mapped units, including glacial and colluvial deposits. Notably, debris flow channels occur on multiple hillslopes above Sitka, and debris flow fan areas (shown in red) extend into developed areas with sensitive infrastructure. This is consistent with the observation that debris flows are the most common type of landslide in Sitka and the surrounding areas in the last ~85 years, including the recent debris flows that initiated in the August 2015 storm. On Harbor Mountain and Gavan Hill, we distinguished a series of debris deposits preserved as triangular wedges of sediment separated by breaks in slope. We display the most prominent of these landforms as the 'sediment wedge' in Figure 5. Notably, hillslopes of the Indian River Valley and on the southeastern face of Mt. Verstovia lack extensive debris flow fans and debris flow deposits.

4.3 | Shallow landslide modelling and validation

Values of q_{cr}/T calculated in our Sitka study region range from 2.34×10^{-5} to 0.71, where lower values indicate greater landslide potential; $\ln(q_{cr}/T)$ values range from −11 to −0.1 with a left-skewed unimodal distribution and a median of −2 (Figure 6b). ('Unconditionally unstable' pixels, where $\frac{q_{cr}}{T} < 0$, are not included in this range. These regions are discussed in detail below.) Colluvial hollows at the head of debris flow channels are particularly susceptible to landsliding and these areas exhibit low values of q_{cr}/T (Figure 6). As demonstrated by studies in unglaciated mountains, regions of low q_{cr}/T are locations where the contributing area is large and topographic convergence in colluvial hollows accumulates colluvium and subsurface flow (Dietrich et al., 2001; Reneau et al., 1990). In the study area, low q_{cr}/T areas occur primarily on the densely dissected mountain fronts directly upslope of Sitka (e.g. Figure 6). Field observations confirm that these areas coincide with very steep hollows and debris flow channels on densely forested hillslopes, where colluvial soils vary in thickness from decimetres to >1 m.

Following Dietrich et al.'s (2001) use of $\ln(q_{cr}/T) < -3.1$ for landslide-prone terrain, we used this threshold to identify the vast

majority of landslide-prone areas; the 5th percentile $\ln(q_{cr}/T) < -3.1$ in 25/38 mapped landslides and only 5/38 landslides occurred where the 5th percentile $\ln(q_{cr}/T) > -3.1$. Eight landslides ($q_{cr}/T < 0$) occurred in unconditionally unstable areas where slope angle is greater than the internal friction angle ($\theta > \varphi$). These slide scarps were not included in statistical analyses because they violated the assumption that hillslopes with slope angles $\theta > 45°$ were unconditionally unstable. Mapped landslide polygons occurred in areas with significantly lower q_{cr}/T values relative to the 200 random distributions (Figure 7a). In fact, Wilcoxon rank sum comparisons of model output for the 30 mapped headscarps and 200 random distributions indicate significant ($p < 0.05$) difference in the distributions. Similarly, a receiver operating characteristic (ROC) curve demonstrates the diagnostic ability of the 5th percentile $\ln(q_{cr}/T)$, with area under the curve (AUC) = 0.709, compared to AUC = 0.5 for random guessing (Figure 7b).

5 | DISCUSSION

5.1 | Landslide occurrence in Southeast Alaska

Previous investigations on the influence of slope aspect on landslide initiation in British Columbia have postulated that glacial flow direction, and the resulting anisotropy in slope angles on different aspects, may control landslide aspect distributions (O'Loughlin, 1972). This process alone cannot explain the distinct pattern of landslide initiation in the TNF, where ice flow directions follow many orientations. The high landslide density on western Baranof and Kruzof islands, particularly on south- and southwest-facing hillslopes, correlates with ocean-facing coastal areas particularly exposed to extreme precipitation and winds as southwesterly atmospheric rivers make landfall (Sharma & Déry, 2019, 2020). Regionally, the western coastline of Southeast Alaska experiences demonstrably higher precipitation rates and hours of non-freezing precipitation than inland areas (Sears-Collins et al., 2006), resulting in higher frequency of the intense rainstorms that trigger landslides. At a more local scale, observed and modelled storm intensities tend to be higher within Sitka Sound as moisture-laden atmosphere is funnelled into the sound by the surrounding topography (Jacobs, 2019, personal communication). These synoptic-scale atmospheric processes correlate with the general trend of high landslide density on western Baranof and Kruzof islands. Conversely, we hypothesize that relatively low landslide density on north- and northeast-facing hillslopes results from a rainshadow effect from southwesterly atmospheric rivers.

5.2 | Geologic setting

The geomorphology of Sitka is influenced by the underlying lithostructural setting as well as glacial and volcanic histories. The geomorphic map presented here is a broadly useful geologic tool that can be used to inform other geomorphic investigations in the study area.

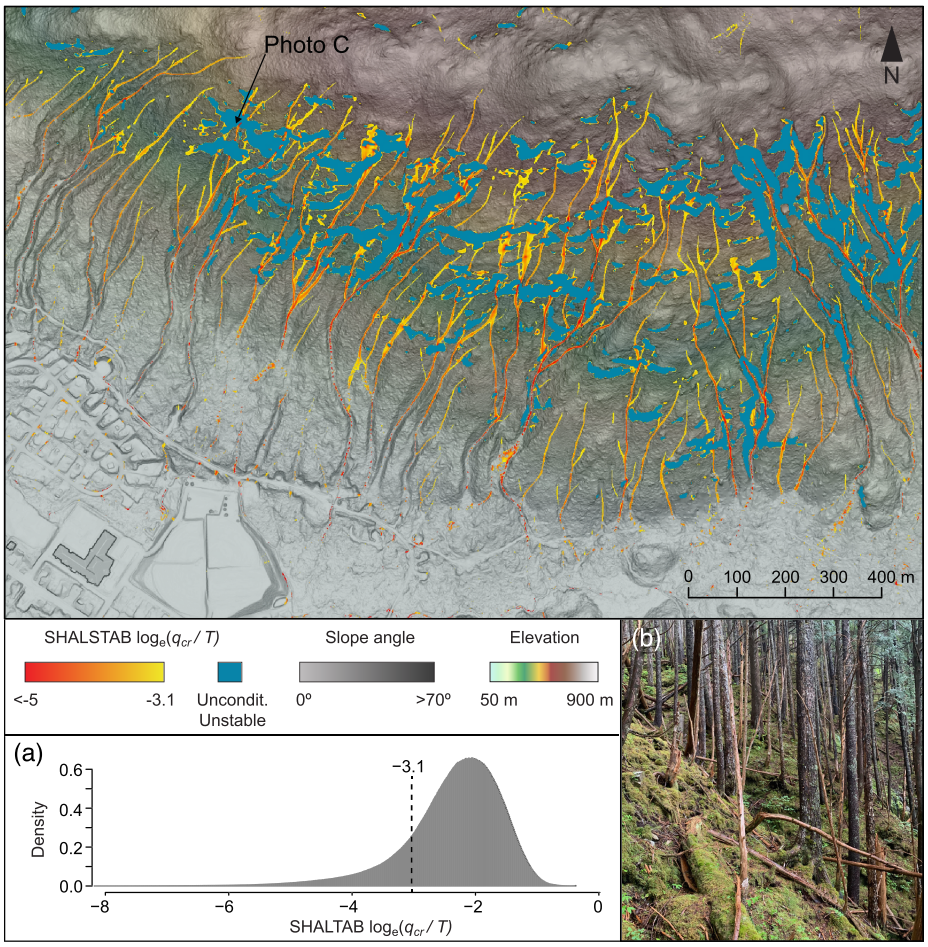

FIGURE 6 Map of q_{cr}/T values for Tsisk'w Googi / Gavan Hill shown on a slope-elevation map. Areas where $\ln(q_{cr}/T) < -3.1$ are shown in yellow and red after the threshold proposed by Dietrich et al. (2001). SHALSTAB results for slopes <25° are not shown because these areas are not prone to shallow landslide initiation. Unconditionally unstable areas correspond to slope angles >45°. In previous validation efforts (e.g. Dietrich et al., 2001) these areas correspond with bedrock cliffs that lack a colluvial mantle. Elevations from 0–900 m are shown as color bands to demonstrate topographic relief. a) Distribution of model output for the entire study area. b) An example of a colluvium-covered steep, convergent hillslope classified as "unconditionally unstable." Unconditionally unstable areas are typically considered too steep to develop soil or accumulate colluvium [Color figure can be viewed at wileyonlinelibrary.com]

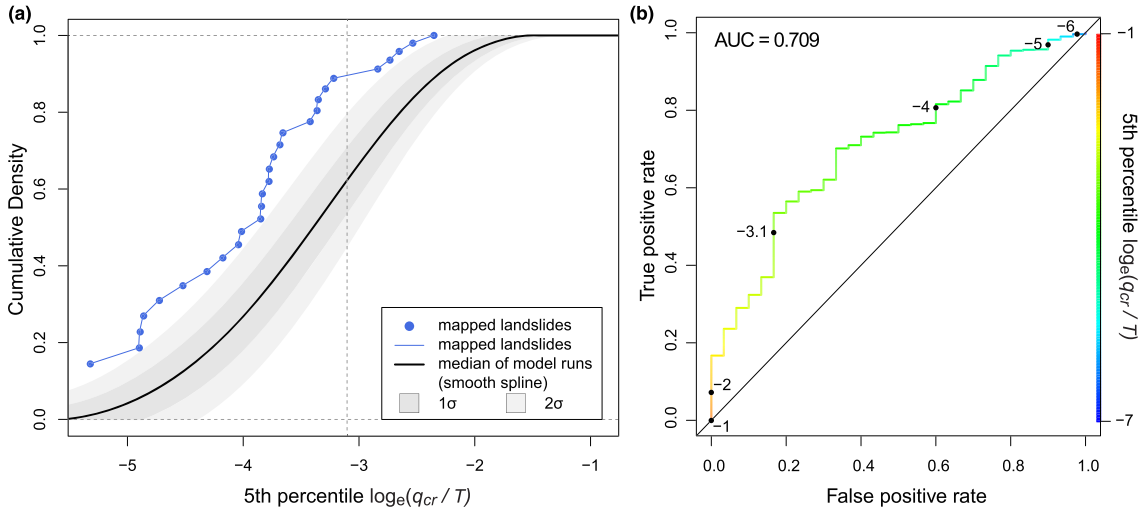

FIGURE 7 (a) Cumulative distribution of 5th percentile SHALSTAB values for each mapped scarp compared to the median 5th percentile SHALSTAB value in 200 random locations in the map area. (b) Receiver Operating Characteristic (ROC) plot showing the efficacy of the SHALSTAB model in classifying landslides compared to 200 random locations. Area under the curve (AUC) is 0.709 compared to AUC = 0.5 for random guessing [Color figure can be viewed at wileyonlinelibrary.com]

Within the Sitka Graywacke Formation (Karl et al., 2015), we refined existing maps by distinguishing a sandy graywacke unit and a cobble conglomerate unit with a series of dextral NW–SE faults. As observed in seismically induced landslides, bedrock weathering along fractures may influence landslide susceptibility (Kargel et al., 2016) by altering rock strength and sediment production (Roy et al., 2016) and controlling hillslope-scale groundwater flow through fractured bedrock (Somers & McKenzie, 2020; Worthington, 2015). Glacial, colluvial, and volcanic sediment creates a complex and locally variable hydrologic system (Figure 5).

Our observations of erosional glacial features and thick (>1 m) deposits of till and outwash throughout the study area are consistent with glacial reconstructions for Southeast Alaska since the Pleistocene. During the late Wisconsin period, locally variable coverage by the margins of the Cordilleran Ice Sheet carved extensive glacial valleys (Kaufman & Manley, 2004; Mann, 1986). As we observed in Sitka, patchy till deposits extend to the tops of many nearby ridges (<800 m), indicating widespread coverage by glacial ice. In Sitka and other areas where glacial topography dominates, over-steepened hillslopes and unconsolidated sediment create landscapes that are susceptible to landslide initiation, particularly debris flows (e.g. Ballantyne, 2002a; Brardinoni et al., 2009; Holm et al., 2004).

In many areas, the 10–11 ka Mt. Edgecumbe tephra deposits (Figure 1a) overlie till, which results in an extreme local gradient of hydraulic conductivity above extremely low-conductivity till. As discussed in detail below, these geomorphic patterns influence the shallow groundwater hydrology that controls landslide initiation.

Channelized hillslopes in Sitka and extensive debris flow fans demonstrate the high hazard potential across large areas in Sitka. The map of debris flow fans deposited since the last glaciation may be used with models of debris flow runout (Booth et al., 2020; Miller, 2019; Shannon and Wilson, Inc., 2016) to evaluate landslide risk to developed areas in Sitka. The geomorphic history of Baranof Island and Sitka Sound influences initiation of landslides with regard to style, susceptibility, and density. Debris flows are the dominant failure style in the historic record in Sitka due to steep postglacial slopes (Brardinoni & Hassan, 2006) and the susceptibility to shallow landslides in small hollows at high elevations (see modelling results).

5.3 | Shallow landslide modelling and validation

The systematic difference in SHALSTAB output between mapped landslides and random distributions demonstrates that debris flows occur in locations of the hillslope that are defined by a set of shared topographic characteristics. These locations are characterized by large contributing areas and topographic convergence, where local (metre-scale) topography routes near-surface groundwater flow and accumulates unconsolidated sediment during precipitation events. The presence of unstable slopes at incised channel heads demonstrates that topography is a first-order control on the initiation of shallow landslides in postglacial landscapes, particularly where reorganization of glacial topography produces linear channels on steep hillsides. Regional investigations in the glaciated mountains of British Columbia have also observed the susceptibility of small colluvial channels (gullies) to shallow landslide initiation (Brardinoni et al., 2003; Brayshaw & Hassan, 2009; Jakob et al., 2005; Millard, 1999).

These modelling results are consistent with the conclusions of studies in unglaciated mountains (Dietrich et al., 2001; Reneau et al., 1990). The efficacy of a simple threshold in identifying landslides demonstrates the applicability of the SHALSTAB model in postglacial landscapes. In particular, the fact that broad patterns in postglacial landslide potential can be identified even with a relatively simple model is encouraging, as more complex models would be difficult or impossible to parameterize (Dietrich et al., 1995; Vieira et al., 2018).

There are limitations to the effective use of SHALSTAB in the study area and other postglacial landscapes. First, field observations indicate that our model may not accurately predict the topographic threshold between colluvium-mantled and bedrock hillslopes. Given

the assigned φ value of 45°, the model incorrectly predicts 'unconditionally unstable' bedrock on several hillslopes where we observed sufficient colluvium to warrant consideration as debris flow initiation sites. Typically, the unconditionally unstable slopes are assumed to indicate bare bedrock slopes or cliffs with little/no potential to initiate shallow landslides. Field observations in Sitka, however, demonstrate that some areas considered unconditionally unstable by the model are in fact mantled by soil and colluvium, and may have a much higher potential to initiate landslides than estimated in this model (Figure 6c). In fact, 8/38 mapped headscarps were located in areas where at least 5% of cells were classified as unconditionally unstable and q_{cr}/T could not be compared with log-transformed randomly located samples. This discrepancy likely results from the extremely dense vegetation in Sitka and Southeast Alaska (Kirchhoff et al., 2016; Van Hees & Mead, 2005), which increases cohesion by roots and stability of steep slopes (e.g. Löbmann et al., 2020).

Without field validation, reliance on the model alone could lead investigators to ignore crucial initiation zones in postglacial landscapes, systematically under-predicting debris flow potential. In Sitka and other landscapes with extremely dense vegetation, our field observations suggest that adjusting the parameters of the model (i.e. increasing the friction angle $\varphi \geq 50°$) could prevent erroneous classification of some unconditionally unstable hillslopes.

Additionally, some mapped debris flows initiated in areas considered relatively stable by the model: five landslides initiated in areas where the 5th percentile $q_{cr}/T > -3.1$. Hillslope-scale analysis of landslide susceptibility has the potential to catastrophically overlook initiation sites that are susceptible to landslides due to locally variable cohesion, lithology, stratigraphy, or hydrologic conditions not captured by the topographic input. Adding spatially explicit cohesion to the model requires the specification of soil depth values across the study area; while this additional complexity tends to improve model performance, it introduces numerous parameters that can be difficult to estimate (e.g. Dietrich et al., 1995; Löbmann et al., 2020). Here, we favour a parsimonious approach that enables us to rapidly and accurately identify potential landslide initiation sites with minimal assumptions and parameterizations.

5.4 | Geomorphic controls on landslide occurrence

Map-scale patterns in several geomorphic variables (tephra distribution and local geomorphology, timber harvest, topography, and climate) correspond to patterns in landslide density and geometry. For example, small landslides occur with high density on northern Kruzof Island, where tephra deposits are 50–200 cm thick, and landslides are smaller and more frequent on Kruzof and western Baranof islands than in many other high-relief areas of Southeast Alaska (Figures 1 and 4). Landslide initiation is strongly influenced by the unique hydrologic properties of stratigraphy dominated by discontinuous tephra soils (Dahlgren et al., 2004; Damiano et al., 2012; Nanzyo, 2002) and glacial deposits. Where extreme gradients in hydraulic conductivity occur (i.e. tephra above till), pore pressure increases along the stratigraphic boundary during storms (Santoso et al., 2011). As we observed in the field, the tephra deposits increase water storage capacity, with large volumes of water present in the soil samples even weeks after a rain event. This storage capacity is likely due to the high porosity, organic concentration, and clay mineral assemblages typical of volcanic soils (Dahlgren et al., 2004; Nanzyo, 2002). These characteristics of volcanic soils influence hillslope susceptibility to landslides (Damiano et al., 2012) by retaining water in micro- and mesopores (Dahlgren et al., 2004) during and after precipitation events. This influence of volcanic soils is associated with susceptibility to landsliding (Bommer et al., 2002; Kluger et al., 2020; Patton et al., 2020). On Kruzof and Baranof islands, the presence of >50 cm-thick Mt. Edgecumbe tephra deposits increases near-surface groundwater storage such that antecedent moisture can be substantial prior to high-intensity rainfall events, resulting in high susceptibility to shallow landslides.

Debris flows in Sitka are typical of steep postglacial hillslopes (Ballantyne, 2019; Ballantyne & Benn, 1994; Hinchliffe & Ballantyne, 2009) and the thin colluvium/tephra soils over till and bedrock are susceptible to shallow landslides that initiate debris flows. In multiple landslides near Sitka, the tephra–till boundary forms the plane of failure that initiates a landslide. For example, the Sawmill Slide (Figure 5b), the South Kramer Slide, and other unnamed landslides in the study area (this study; Booth et al., 2020; Landwehr et al., 2016) initiated along the tephra–till interface. Landslide initiation along the surface of low-permeability till has been observed in other postglacial landscapes, including Ireland (Dykes et al., 2008), Washington State, USA (Heller, 1981), and Norway (Carey, 2018). In these examples, slow infiltration rates in till deposits result in an extreme contrast in hydraulic conductivity between till and the overlying material. Furthermore, the strength contrast between till and overlying tephra is large, with relatively low shear strength in saturated clay-rich volcanic sediment (Behnsen & Faulkner, 2012). Thus, when landslides initiate, they are particularly likely to fail along the tephra–till boundary.

In some regions of the TNF, areas of documented timber harvest since 1900 also have a higher density of landslides (Figure 1b). Previous investigations document how timber harvest history influences debris flow initiation and typical runout lengths, with recently clear-cut hillslopes more susceptible to erosion by debris flows (Bishop & Stevens, 1964; Gomi et al., 2004; Johnson et al., 2000; Swanston & Marion, 1991). As observed on Prince of Wales Island, landslides in very recently logged areas (1–3 years) tend to be smaller and more frequent. Notably, mapping bias in less dense forests may exaggerate this pattern at a map scale (Brardinoni et al., 2003). Even in areas without recent timber harvest, stand age influences landslide mobility and runout lengths, with younger forests characterized by longer runout (Booth et al., 2020).

Disproportionate landslide occurrence on south- and southwest-facing hillslopes in Southeast Alaska (Figure 3) follows observed climatic patterns: the ARs that deliver most extreme precipitation to coastal Southeast Alaska are dominated by south and southwesterly winds. Microclimate variability, including metrics of precipitation and windspeed, is also influential in controlling individual landslide initiation during storms (Buma & Johnson, 2015; Minder et al., 2009).

Spatial coincidence of these driving variables in our study area hinders quantification of their individual role in landslide initiation. Nevertheless, we can recognize that all of these factors can influence landslide initiation, and the increase in landslide susceptibility is greatest where these variables overlap. For example, landslide density is high on the southwest-facing slopes of Baranof Island, even to the south of the mapped Mt. Edgecumbe tephra extent. The highest landslide densities on the island, however, are in Sitka Sound, where

tephra deposits are 50–200 cm thick and where slope aspects are primarily south–southwest. Direct observations of landslides in this area confirm that several landslides have initiated along the tephra–till boundary. Similarly, spatial correlation between landslide density and logging activity on Chicagof and Prince of Wales islands (Figure 1b) corroborates previous investigations which concluded that timber harvest increases the frequency of small landslides in Southeast Alaska (Gomi et al., 2004; Johnson et al., 2000; Swanston & Marion, 1991). Of these logged areas, landslide density is particularly high on Kruzof Island, where historic logging coincides with thick (200 cm) tephra deposits (Figures 1a and b). To effectively characterize landslide processes in an extremely heterogeneous landscape, these correlated geomorphic controls must be considered holistically.

6 | CONCLUSIONS

Landslides are prevalent throughout Southeast Alaska and tend to occur following extreme precipitation (ARs). First-order geomorphic controls on landslide initiation include glacial and volcanic history, topography (e.g. steep slopes, large contributing area, southwestern aspect), timber harvest, and climate, although the relative contributions of these controls remain unclear. A high density of small, frequent landslides on western Baranof and Kruzof islands corresponds to regions where patchy distribution of porous volcanic soils overlies impermeable till. The till–tephra interface is a typical failure plane of landslides near Sitka due to the extreme gradient of hydraulic conductivity and strength.

Similarly, the topographically based shallow landslide model SHALSTAB characterized unstable hillslopes using high-resolution (1 m) topographic data. Metre-scale anomalies in curvature and contributing area correlate to mapped landslides. Hillslopes with $\ln(q_{cr}/T) < -3.1$ are more susceptible to landslides. The model outperforms random guessing (ROC AUC = 0.709 vs. 0.5). SHALSTAB effectively characterized unstable hillslopes in a postglacial landscape without explicitly accounting for the extreme local heterogeneity in substrate characteristics like cohesion and transmissivity. The success of this model demonstrates that simple topographic models are a useful tool for evaluating shallow landslide initiation in postglacial landscapes. A limitation of the model in glacial terrain is its ability to predict the threshold between colluvium-mantled hillslopes and 'unconditionally unstable' bedrock hillslopes with low landslide potential.

ACKNOWLEDGEMENTS

This work was funded by National Science Foundation Award #1831770. The Sitka Sound Science Center (SSSC) provided project planning and logistic support. We thank Robert Lempert and Ryan Brown (RAND Corporation) and Lisa Busch (SSSC) for project management and Jeff Feldspauch, Tammy Young, and Liz Borneman (Sitka Tribe of Alaska) for collaboration and cultural resources. We also sincerely thank Ben Mirus and Corina Cerovski-Darriau (USGS), Aaron Jacobs (NWS), Aaron Prussian, KK Prussian, and Jacquie Foss (USFS), Oscar Roering, Robert Woolsey (KCAW Radio), and Robin Kim and Cora Siebert (SSSC) for contributing ideas and field support. The authors have no conflicts of interest. The Tlingit people have been indigenous to this land for over 10 000 years. Gunalchéesh to the Tlingit people for their stewardship of Lingít Aaní since time immemorial and today.

DATA AVAILABILITY STATEMENT

Data that support the findings of this study are available from the US Forest Service, Tongass National Forest (https://hub.arcgis.com/datasets/e2f7e4b47b434f1c873ac3278717f801_0?geometry=92.621%2C48.763%2C113.528%2C51.234) and the Alaska Division of Geology and Geophysical Surveys (https://doi.org/10.14509/30531).

ORCID

Annette I. Patton https://orcid.org/0000-0002-8841-1925
Joshua J. Roering https://orcid.org/0000-0003-0647-3338
Elijah Orland https://orcid.org/0000-0001-8347-3951

REFERENCES

Ager, T.A., Carrara, P.E., Smith, J.L., Anne, V. & Johnson, J. (2010) Postglacial vegetation history of Mitkof Island, Alexander Archipelago, southeastern Alaska. *Quaternary Research*, 73(2), 259–268. Available from: https://doi.org/10.1016/j.yqres.2009.12.005

Ballantyne, C.K. (2002a) A general model of paraglacial landscape response. *The Holocene*, 12(3), 371–376. Available from: https://doi.org/10.1191/0959683602hl553fa

Ballantyne, C.K. (2002b) Paraglacial geomorphology. *Quaternary Science Reviews*, 21, 1935–2007.

Ballantyne, C.K. (2019) After the ice: Lateglacial and Holocene landforms and landscape evolution in Scotland. *Earth and Environmental Science Transactions of the Royal Society of Edinburgh*, 110, 133–171.

Ballantyne, C.K. & Benn, D.I. (1994) Paraglacial slope adjustment and resedimentation following recent glacier retreat, Fabergstolsdalen, Norway. *Arctic & Alpine Research*, 26(3), 255–269. Available from: https://doi.org/10.2307/1551938

Behnsen, J. & Faulkner, D.R. (2012) The effect of mineralogy and effective normal stress on frictional strength of sheet silicates. *Journal of Structural Geology*, 42, 49–61. Available from: https://doi.org/10.1016/j.jsg.2012.06.015

Benda, L. & Dunne, T. (1997) Stochastic forcing of sediment supply to channel networks from landsliding and debris flow. *Water Resources Research*, 33(12), 2849–2863. Available from: https://doi.org/10.1029/97WR02388

Bishop, D.M. & Stevens, M.E. (1964) *Landslides on Logged Areas in SE Alaska*. USDA Forest Service Paper N0R-I. U.S. Department of Agriculture: Juneau, AL.

Bommer, J.J., Rolo, R., Mitroulia, A. & Berdousis, P. (2002) Geotechnical properties and seismic slope stability of volcanic soils. In *Proceedings of the 12th European Conference on Earthquake Engineering*. London.

Booth, A.M., Sifford, C., Vascik, B., Siebert, C. & Buma, B. (2020) Large wood inhibits debris flow runout in forested southeast Alaska. *Earth Surface Processes and Landforms*, 45(7), 1555–1568. Available from: https://doi.org/10.1002/esp.4830

Bovis, M.J. & Jakob, M. (1999) The role of debris supply conditions in predicting debris flow activity. *Earth Surface Processes and Landforms*, 24, 1039–1054. Available from: https://doi.org/10.1002/(SICI)1096-9837(199910)24:11<1039::AID-ESP29>3.0.CO;2-U

Brardinoni, F., Church, M., Simoni, A. & Macconi, P. (2012) Lithologic and glacially conditioned controls on regional debris-flow sediment dynamics. *Geology*, 40(5), 455–458. Available from: https://doi.org/10.1130/G33106.1

Brardinoni, F. & Hassan, M.A. (2006) Glacial erosion, evolution of river long profiles, and the organization of process domains in mountain drainage basins of coastal British Columbia. *Journal of Geophysical Research, Earth Surface*, 111(F1), 1–12. Available from: https://doi.org/10.1029/2005JF000358

Brardinoni, F., Hassan, M.A., Rollerson, T. & Maynard, D. (2009) Colluvial sediment dynamics in mountain drainage basins. *Earth and Planetary Science Letters*, 284(3–4), 310–319. Available from: https://doi.org/10.1016/j.epsl.2009.05.002

Brardinoni, F., Slaymaker, O. & Hassan, M.A. (2003) Landslide inventory in a rugged forested watershed: A comparison between air-photo and

field survey data. *Geomorphology*, 54(3–4), 179–196. Available from: https://doi.org/10.1016/S0169-555X(02)00355-0

Brayshaw, D. & Hassan, M.A. (2009) Debris flow initiation and sediment recharge in gullies. *Geomorphology*, 109(3–4), 122–131. Available from: https://doi.org/10.1016/j.geomorph.2009.02.021

Buma, B. & Johnson, A.C. (2015) The role of windstorm exposure and yellow cedar decline on landslide susceptibility in Southeast Alaskan temperate rainforests. *Geomorphology*, 228, 504–511. Available from: https://doi.org/10.1016/j.geomorph.2014.10.014

Busch, L., Foss, J., Prussian, K., Landwehr, D., Hoffman, J., Becker, M., Gould, A., Wolken, G., Stevens, D.A., Whorton, E., Fielding, E., Buma, B., Carter, B. & Sitka Geotask Force (2016) Sitka Geotask Force Summaries: August 2015 Sitka Landslides.

Campbell, D. & Church, M. (2003) Reconnaissance sediment budgets for Lynn Valley, British Columbia: Holocene and contemporary time scale. *Canadian Journal of Earth Sciences*, 40(5), 701–713. Available from: https://doi.org/10.1139/e03-012

Campbell, S., van Hees, W.W.S. & Mead, B. (2004) *Southeast Alaska Forests: Inventory Highlights*. U.S. Department of Agriculture, Forest Service, Pacific Northwest Research Station: Anchorage, AK.

Carey, G.R. (2018) *Back-analysis study of selected Norwegian debris flow and debris avalanche events: A comparison of DAN3D and GeoClaw*. Master's thesis, University of Oslo.

Chae, B.-G., Park, J.-J., Catani, F., Simoni, A. & Berti, M. (2017) Landslide prediction, monitoring and early warning: A concise review of state-of-the-art. *Geosciences Journal*, 21(6), 1033–1070. Available from: https://doi.org/10.1007/s12303-017-0034-4

Coe, J.A. & Godt, J.W. (2012) Review of approaches for assessing the impact of climate change onlandslide hazards. In: Eberhardt, E., Froese, C., Turner, K. & Leroueil, S. (Eds.) *Landslides and Engineered Slopes: Protecting Society through Improved Understanding*. London: Taylor & Francis, pp. 371–377.

Compton, R.R. (1985) *Geology in the Field*. Chichester: Wiley.

Cordeira, J.M., Stock, J., Dettinger, M.D., Young, A.M., Kalansky, J.F. & Ralph, F.M. (2019) A 142-year climatology of northern California landslides and atmospheric rivers. *Bulletin of the American Meteorological Society*, 100(8), 1499–1509. Available from: https://doi.org/10.1175/BAMS-D-18-0158.1

Cruden, D.M. & Varnes, D.J. (1996) Landslide types and processes. Transportation Research Board, U.S. National Academy of Sciences. Special Report, 247, 36–75

Daanen, R.P., Wolken, G.J. & Herbst, A.M. (2020) *LiDAR-derived elevation data for Sitka, Alaska*. Raw Data File 2020–13: State of Alaska Division of Geological & Geophysical Surveys.

Dahlgren, R.A., Saigusa, M. & Ugolini, F.C. (2004) The nature, properties, and management of volcanic soils. *Advances in Agronomy*, 82, 113–182. Available from: https://doi.org/10.1016/S0065-2113(03)82003-5

Damiano, E., Olivares, L. & Picarelli, L. (2012) Steep-slope monitoring in unsaturated pyroclastic soils. *Engineering Geology*, 137–138, 1–12. Available from: https://doi.org/10.1016/j.enggeo.2012.03.002

DiBiase, R.A., Lamb, M.P., Ganti, V. & Booth, A.M. (2017) Slope, grain size, and roughness controls on dry sediment transport and storage on steep hillslopes. *Journal of Geophysical Research, Earth Surface*, 122(4), 941–960. Available from: https://doi.org/10.1002/2016JF003970

Dietrich, W.E., Bellugi, D. & Real de Asua, R. (2001) Validation of the shallow landslide model, SHALSTAB, for forest management. *Land Use and Watersheds: Human Influence on Hydrology and Geomorphology in Urban and Forest Areas*, 2, 195–227. Available from: https://doi.org/10.1029/ws002p0195

Dietrich, W.E. & Dunne, T. (1978) Sediment budget for a small catchment in mountainous terrain. *Zeitschrift für Geomorphologie*, 29, 191–206. Available from: https://doi.org/10.1130/0091-7613(2001)029

Dietrich, W.E., Reiss, R., Hsu, M. & Mongtomery, D.R. (1995) A process-based model for colluvial soil depth and shallow landsliding using digital elevation data. *Hydrological Processes*, 3–4, 383–400.

Dykes, A.P., Gunn, J. & Convery, K.J. (2008) Landslides in blanket peat on Cuilcagh Mountain, northwest Ireland. *Geomorphology*, 102(3–4), 325–340. Available from: https://doi.org/10.1016/j.geomorph.2008.04.003

Elliott, J. & Freymueller, J.T. (2020) A block model of present-day kinematics of Alaska and Western Canada. *Journal of Geophysical Research, Solid Earth*, 125(7), 1–30. Available from: https://doi.org/10.1029/2019JB018378

Gomi, T., Sidle, R.C. & Swanston, D.N. (2004) Hydrogeomorphic linkages of sediment transport in headwater streams, Maybeso Experimental Forest, Southeast Alaska. *Hydrological Processes*, 18(4), 667–683. Available from: https://doi.org/10.1002/hyp.1366

Greco, R., Guida, A., Damiano, E. & Olivares, L. (2010) Soil water content and suction monitoring in model slopes for shallow flowslides early warning applications. *Physics and Chemistry of the Earth*, 35(3–5), 127–136. Available from: https://doi.org/10.1016/j.pce.2009.12.003

Hamilton, T.D. (1986) Correlation of quaternary glacial deposits in Alaska. *Quaternary Science Reviews*, 5, 171–180. Available from: https://doi.org/10.1016/0277-3791(86)90182-4

Harris, A.S. (1999) *Wind in the Forests of Southeast Alaska and Guides for Reducing Damage*. USDA General Technial Report. U.S. Department of Agriculture, Forest Service, Pacific Northwest Research Station: Portland, OR.

Harris, A.S. & Farr, W.A. (1974) *The forest ecosystem of Southeast Alaska*. Available from: http://www.fs.fed.us/pnw/publications/pnw_gtr025/pnw_gtr025a.pdf

Heller, P.L. (1981) Small landslide types and controls in glacial deposits: Lower Skagit river drainage, northern cascade range, Washington. *Environmental Geology*, 3(4), 221–228. Available from: https://doi.org/10.1007/BF02473506

Heuer, P. (2020) *Personal communication: Silviculturalist*. U.S. Forest Service, Tongass National Forest: Ketchikan, AK.

Hinchliffe, S. & Ballantyne, C.K. (2009) Talus structure and evolution on sandstone mountains in NW Scotland. *Holocene*, 19(3), 477–486. Available from: https://doi.org/10.1177/0959683608101396

Holm, K., Bovis, M. & Jakob, M. (2004) The landslide response of alpine basins to post-Little Ice Age glacial thinning and retreat in southwestern British Columbia. *Geomorphology*, 57(3–4), 201–216. Available from: https://doi.org/10.1016/S0169-555X(03)00103-X

Hungr, O., Leroueil, S. & Picarelli, L. (2014) The Varnes classification of landslide types, an update. *Landslides*, 11(2), 167–194. Available from: https://doi.org/10.1007/s10346-013-0436-y

Hungr, O., McDougall, S. & Bovis, M. (2005) Entrainment of material by debris flows. In: Jakob, M. & Hungr, O. (Eds.) *Debris-Flow Hazards and Related Phenomena*. Chichester: Springer/Praxis, pp. 135–158.

Iverson, R.M. (1997) The physics of debris flows. *Reviews of Geophysics*, 35(3), 245–296. Available from: https://doi.org/10.1029/97RG00426

Jacobs, A. (2019) *Personal communication: Atmospheric Scientist*. National Weather Service: Juneau, AL.

Jacobs, A. (2020) *Haines Weather/Data Summary for Debris Flows, Landslides, Flooding Event*. Juneau, AL: Weather Forecast Office.

Jacobs, A., Holloway, E. & Dixon, A. (2016) Atmospheric rivers in Alaska – yes they do exist, and are usually tied to the biggest and most damaging rain-generated floods in Alaska. In *Proceedings of the 2016 International Atmospheric Rivers Conference*, La Jolla, CA.

Jakob, M., Bovis, M. & Oden, M. (2005) The significance of channel recharge rates for estimating debris-flow magnitude and frequency. *Earth Surface Processes and Landforms*, 30(6), 755–766. Available from: https://doi.org/10.1002/esp.1188

Johnson, A.C., Swanston, D.N. & McGee, K.E. (2000) Landslide initiation, runout, and deposition within clearcuts and old-growth forests of Alaska. *Journal of the American Water Resources Association*, 36(1), 17–30. Available from: https://doi.org/10.1111/j.1752-1688.2000.tb04245.x

Juneau Local Emergency Planning Commitee. (2009) All-Hazards Mitigation Plan: The City and Borough of Juneau. https://juneau.org/wp-content/uploads/2017/08/All-Hazards-Mitigation-Plan.pdf#:~:text=The%20City%20and%20Borough%20of%20Juneau%20(CBJ)%20All-Hazards,that%20may%20help%20the%20CBJ%20prevent%20disaster%20losses

Kargel, J.S., Leonard, G.J., Shugar, D.H., Haritashya, U.K., Bevington, A., Fielding, E.J. et al. (2016) Geomorphic and geologic controls of geohazards induced by Nepal's 2015 Gorkha earthquake. *Science*, 351, 1–8. Available from: https://doi.org/10.1126/science.aac8353

Karl, S.M., Haeussler, P.J., Himmelberg, G.R., Zumsteg, C.L. Layer, P.W., Friedman, R.M., Roeske, S.M. & Snee, L.W. (2015) *Geologic map of Baranof Island, Southeast Alaska*. U.S. Geological Survey Scientific Investigations Map 3335, scale 1:200,000.

Kaufman, D.S. & Manley, W.F. (2004) Pleistocene Maximum and Late Wisconsinan glacier extents across Alaska, U.S.A. *Developments in Quaternary Science*, 2, 9–27. Available from: https://doi.org/10.1016/S1571-0866(04)80182-9

Kirchhoff, M., Smith, M. & Walker, N. (2016) Land cover & forest vegetation. In: *Ecological Atlas of Southeast Alaska*. Anchorage, AK: Audubon Alaska, pp. 44–49.

Kluger, M.O., Jorat, E.M., Moon, V.G., Kreiter, S., de Lange, W.P., Mörz, T., Robertson, T. & Lowe, D.J. (2020) Rainfall threshold for initiating effective stress decrease and failure in weathered tephra slopes. *Landslides*, 17(2), 267–281. Available from: https://doi.org/10.1007/s10346-019-01289-2

Lamb, M.P., Levina, M., Dibiase, R.A. & Fuller, B.M. (2013) Sediment storage by vegetation in steep bedrock landscapes: Theory, experiments, and implications for postfire sediment yield. *Journal of Geophysical Research, Earth Surface*, 118(2), 1147–1160. Available from: https://doi.org/10.1002/jgrf.20058

Landwehr, D.J., Foss, J.V., Prussian, K. & Johnson, A. (2016) Investigations of landslides in the Sitka area caused by the September 19th 2014 and August 18th 2015 storm events.

Lavers, D.A., Ralph, F.M., Neiman, P.J., Wick, G.A., Scott, C.A., McCollor, D. & White, T. (2014) Atmospheric rivers in Southeast Alaska and British Columbia: The Bella Coola event of 2010 and Alaska events of 2012. In *Proceedings of the AGU Fall Meeting*, San Francisco, CA.

Lesnek, A.J., Briner, J.P., Lindqvist, C., Baichtal, J.F. & Heaton, T.H. (2018) Deglaciation of the Pacific coastal corridor directly preceded the human colonization of the Americas. *Science Advances*, 4, eaar5040. Available from: https://doi.org/10.1126/sciadv.aar5040

Löbmann, M.T., Geitner, C., Wellstein, C. & Zerbe, S. (2020) The influence of herbaceous vegetation on slope stability – a review. *Earth-Science Reviews*, 209, 103328. Available from: https://doi.org/10.1016/j.earscirev.2020.103328

Mann, D.H. (1986) Wisconsin and Holocene glaciation of Southeast Alaska: Glaciation in Alaska. *The Geologic Record*, 64, 237–265. Available from: https://doi.org/10.4018/978-1-60566-198-8.ch103

Mann, D.H. & Hamilton, T.D. (1995) Late Pleistocene and Holocene paleoenvironments of the North Pacific coast. *Quaternary Science Reviews*, 14(5), 449–471. Available from: https://doi.org/10.1016/0277-3791(95)00016-I

Martin, Y., Rood, K., Schwab, J.W. & Church, M. (2002) Sediment transfer by shallow landsliding in the Queen Charlotte Islands, British Columbia. *Canadian Journal of Earth Sciences*, 39(2), 189–205. Available from: https://doi.org/10.1139/e01-068

Millard, T. (1999) *Debris Flow Initiation in Coastal British Columbia Gullies*, Forest Research Technical Report TR-002. Victoria, BC: Canadian Forest Service.

Miller, D. (2019) Modeling Susceptibility to Landslides and Debris Flows in Southeast: TerrainWorks Report to the U.S. Forest Service, Tongass National Forest. https://terrainworks.sharefile.com/share/view/s5df33105ae3a4eb8a3895b93cba01188

Miller, D.J. & Burnett, K.M. (2008) A probabilistic model of debris-flow delivery to stream channels, demonstrated for the Coast Range of Oregon, USA. *Geomorphology*, 94, 184–205. Available from: https://doi.org/10.1016/j.geomorph.2007.05.009

Milne, F.D., Brown, M.J., Davies, M.C.R. & Cameron, G. (2015) Some key topographic and material controls on debris flows in Scotland. *Quarterly Journal of Engineering Geology and Hydrogeology*, 48(3–4), 212–223. Available from: https://doi.org/10.1144/qjegh2013-095

Minder, J.R., Roe, G.H. & Montgomery, D.R. (2009) Spatial patterns of rainfall and shallow landslide susceptibility. *Water Resources Research*, 45(4), 1–11. Available from: https://doi.org/10.1029/2008WR007027

Montgomery, D.R. & Dietrich, W.E.E. (1994) A physically based model for the hydrologic control on shallow landsliding. *Water Resources Research*, 30(6), 1153–1171. Available from: https://doi.org/10.1029/2005WR004369

Nanzyo, M. (2002) Unique properties of volcanic ash soils. *Global Journal of Environmental Research*, 6, 99–112.

Neiman, P.J., Ralph, F.M., Wick, G.A., Lundquist, J.D. & Dettinger, M.D. (2008) Meteorological characteristics and overland precipitation impacts of atmospheric rivers affecting the west coast of North America based on eight years of SSM/I satellite observations. *Journal of Hydrometeorology*, 9(1), 22–47. Available from: https://doi.org/10.1175/2007JHM855.1

Neiman, P.J., Schick, L.J., Martin Ralph, F., Hughes, M. & Wick, G.A. (2011) Flooding in western Washington: The connection to atmospheric rivers. *Journal of Hydrometeorology*, 12(6), 1337–1358. Available from: https://doi.org/10.1175/2011JHM1358.1

Oakley, N.S., Lancaster, J.T., Kaplan, M.L. & Ralph, F.M. (2017) Synoptic conditions associated with cool season post-fire debris flows in the Transverse Ranges of Southern California. *Natural Hazards*, 88(1), 327–354. Available from: https://doi.org/10.1007/s11069-017-2867-6

O'Loughlin, C.L. (1972) *An investigation of the stability of the steepland forest soils in the coast mountains, Southwest, British Columbia*. PhD thesis, University of British Columbia.

Patton, A.I., Rathburn, S.L. & Capps, D.M. (2019) Landslide response to climate change in permafrost regions. *Geomorphology*, 340, 116–128. Available from: https://doi.org/10.1016/j.geomorph.2019.04.029

Patton, A.I., Rathburn, S.R., Capps, D., Brown, R.A. & Singleton, J.S. (2020) Lithologic, geomorphic, and permafrost controls on recent landsliding in the Alaska Range. *Geosphere*, 16, 1479–1494. Available from: https://doi.org/10.1130/ges02256.1

Ralph, F.M., Neiman, P.J. & Wick, G.A. (2004) Satellite and CALJET aircraft observations of atmospheric rivers over the Eastern North Pacific Ocean during the winter of 1997/98. *Monthly Weather Review*, 132(7), 1721–1745. Available from: https://doi.org/10.1175/1520-0493(2004)132<1721:SACAOO>2.0.CO;2

Reneau, S.L., Dietrich, W.E., Donahue, D.J., Jull, J.T. & Rubin, M. (1990) Late Quaternary history of colluvial deposition and erosion in hollows, Central California Coast Ranges. *Geological Society of America Bulletin*, 102, 969–982. Available from: https://doi.org/10.1130/0016-7606(1990)102<0969

Riehle, J.R., Champion, D.E., Brew, D.A. & Lanphere, M.A. (1992a) Pyroclastic deposits of the Mount Edgecumbe volcanic field, Southeast Alaska: Eruptions of a stratified magma chamber. *Journal of Volcanology and Geothermal Research*, 53(1–4), 117–143. Available from: https://doi.org/10.1016/0377-0273(92)90078-R

Riehle, J.R., Mann, D.H., Peteet, D.M., Engstrom, D.R., Brew, D.A. & Meyer, C.E. (1992b) The Mount Edgecumbe tephra deposits, a marker horizon in southeastern Alaska near the Pleistocene–Holocene boundary. *Quaternary Research*, 37(2), 183–202. Available from: https://doi.org/10.1016/0033-5894(92)90081-S

Roy, S.G., Tucker, G.E., Koons, P.O., Smith, S.M. & Upton, P. (2016) A fault runs through it: Modeling the influence of rock strength and grain-size distribution in a fault-damaged landscape. *Journal of Geophysical Research, Earth Surface*, 121(10), 300–316. Available from: https://doi.org/10.1002/2015JF003662

Sandberg, E. (2013) *A History of Alaska Population Settlement*. Alaska Department of Labor and Workforce Development: Juneau, AK.

Santoso, A.M., Phoon, K.K. & Quek, S.T. (2011) Effects of soil spatial variability on rainfall-induced landslides. *Computers and Structures*, 89(11–12), 893–900. Available from: https://doi.org/10.1016/j.compstruc.2011.02.016

Schuster, R.L. & Highland, L.M. (2007) Overview of the effects of mass wasting on the natural environment. *Environmental and Engineering Geoscience*, 13(1), 25–44. Available from: https://doi.org/10.2113/gseegeosci.13.1.25

Sears-Collins, A.L., Schultz, D.M. & Johns, R.H. (2006) Spatial and temporal variability of nonfreezing drizzle in the United States and Canada.

Journal of Climate, 19(15), 3629–3639. Available from: https://doi.org/10.1175/JCLI3796.1

Shannon and Wilson, Inc. (2016) *South Kramer Avenue Landslide: Jacobs Circle to Emmons Street*. https://www.cityofsitka.com/documents/Sitka_SKramerLandslideReport.pdf

Sharma, A.R. & Déry, S.J. (2019) Variability and trends of landfalling atmospheric rivers along the Pacific Coast of northwestern North America. *International Journal of Climatology*, 40(1), 1–15. Available from: https://doi.org/10.1002/joc.6227

Sharma, A.R. & Déry, S.J. (2020) Contribution of atmospheric rivers to annual, seasonal, and extreme precipitation across British Columbia and southeastern Alaska. *Journal of Geophysical Research – Atmospheres*, 125(9), 1–21. Available from: https://doi.org/10.1029/2019jd031823

Somers, L.D. & McKenzie, J.M. (2020) A review of groundwater in high mountain environments. *Wiley Interdisciplinary Reviews Water*, 7(6), 1–27. Available from: https://doi.org/10.1002/wat2.1475

Stark, C.P. & Hovius, N. (2001) The characterization of landslide size distributions. *Geophysical Research Letters*, 28(6), 1091–1094. Available from: https://doi.org/10.1029/2000GL008527

Steger, S., Brenning, A., Bell, R. & Glade, T. (2017) The influence of systematically incomplete shallow landslide inventories on statistical susceptibility models and suggestions for improvements. *Landslides*, 14(5), 1767–1781. Available from: https://doi.org/10.1007/s10346-017-0820-0

Stock, J. & Dietrich, W.E. (2003) Valley incision by debris flows: Evidence of a topographic signature. *Water Resources Research*, 39(4), 1–25. Available from: https://doi.org/10.1029/2001WR001057

Stock, J.D. & Dietrich, W.E. (2006) Erosion of steepland valleys by debris flows. *Bulletin of the Geological Society of America*, 118(9–10), 1125–1148. Available from: https://doi.org/10.1130/B25902.1

Swanston, D.N. & Marion, D.A. (1991) Landslide response to timber harvest in Southeast Alaska. In *Proceedings of the 5th Federal Interagency Sedimentation Conference*, Las Vegas, NV.

Tongass National Forest. (n.d.) *Tongass landslide areas*. USDA Forest Service Vector Digital Data.

Turner, T.R., Duke, S.D., Fransen, B.R., Reiter, M.L., Kroll, A.J., Ward, J.W., Bach, J.L., Justice, T.E. & Bilby, R.E. (2010) Landslide densities associated with rainfall, stand age, and topography on forested landscapes, southwestern Washington, USA. *Forest Ecology and Management*, 259(12), 2233–2247. Available from: https://doi.org/10.1016/j.foreco.2010.01.051

Twenhofel, W.S. (1951) *Geology of Proposed Blue Lake Dam Site*, USGS Circular 147. Reston, VA: U.S. Geological Survey.

USGS Standards. (2020) *Gems (Geologic map schema)—a standard format for the digital publication of geologic maps*. U.S. Geological Survey Techniques and Methods, v. 2020.

Van Hees, W.W.S. & Mead, B.R. (2005) Extensive, strategic assessment of southeast Alaska's vegetative resources. *Landscape and Urban Planning*, 72(1–3), 25–48. Available from: https://doi.org/10.1016/j.landurbplan.2004.09.027

Varnes, D.J. (1978) Slope movement types and processes. *Landslides*, 176, 11–33.

Vieira, B.C., Fernandes, N.F., Augusto Filho, O., Martins, T.D. & Montgomery, D.R. (2018) Assessing shallow landslide hazards using the TRIGRS and SHALSTAB models, Serra do Mar, Brazil. *Environmental Earth Sciences*, 77(6), 1–15. Available from: https://doi.org/10.1007/s12665-018-7436-0

Wendler, G., Galloway, K. & Stuefer, M. (2016) On the climate and climate change of Sitka, Southeast Alaska. *Theoretical and Applied Climatology*, 126(1–2), 27–34. Available from: https://doi.org/10.1007/s00704-015-1542-7

White, C., Gehrels, G.E., Pecha, M., Giesler, D., Yokelson, I., McClelland, W.C. & Butler, R.F. (2016) U-Pb and Hf isotope analysis of detrital zircons from Paleozoic strata of the southern Alexander terrane (Southeast Alaska). *Lithosphere*, 8(1), 83–96. Available from: https://doi.org/10.1130/L475.1

Worthington, S.R.H. (2015) Diagnostic tests for conceptualizing transport in bedrock aquifers. *Journal of Hydrology*, 529, 365–372. Available from: https://doi.org/10.1016/j.jhydrol.2015.08.002

How to cite this article: Patton, A.I., Roering, J.J. & Orland, E. (2022) Debris flow initiation in postglacial terrain: Insights from shallow landslide initiation models and geomorphic mapping in Southeast Alaska. *Earth Surface Processes and Landforms*, 47(6), 1583–1598. Available from: https://doi.org/10.1002/esp.5336